Analysis of the Cu-Al Milling Stages Through the Microstructure Evolution Studied by TEM and SEM

M. F. Giordana, N. Muñoz-Vásquez, M. R. Esquivel & E. Zelaya

Metallography, Microstructure, and Analysis
Application and Innovation for Metals, Alloys, and Engineered Materials

ISSN 2192-9262

Metallogr. Microstruct. Anal.
DOI 10.1007/s13632-017-0339-8

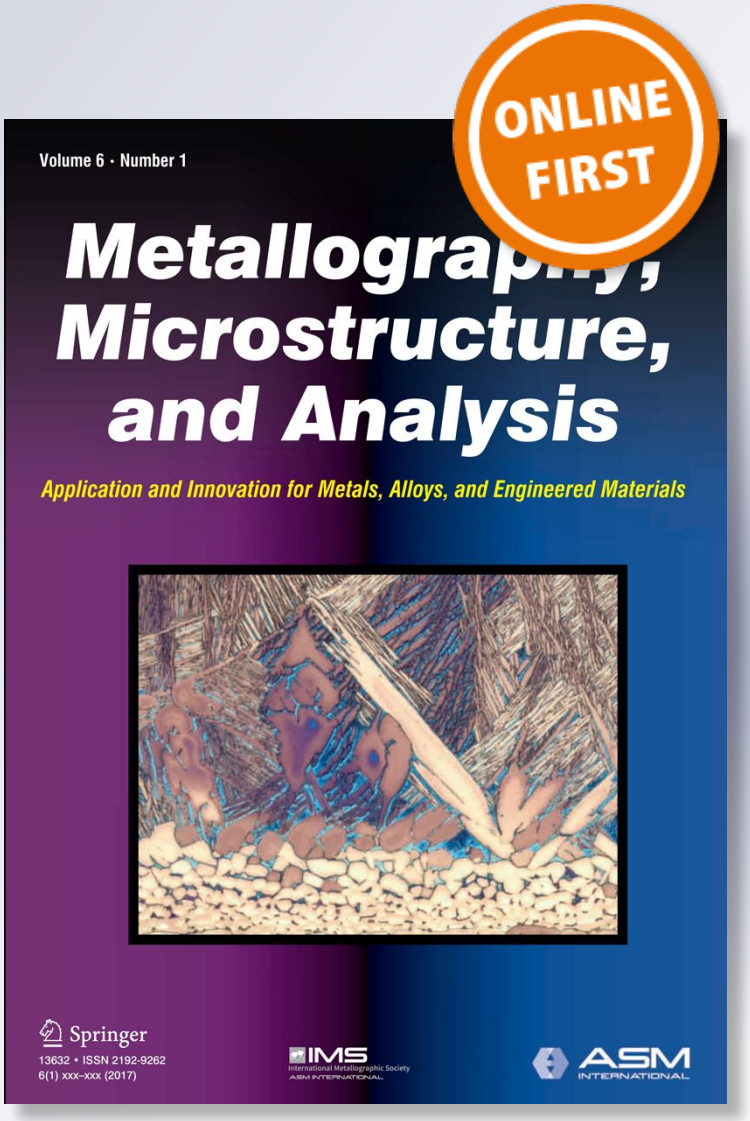

Springer

Metallogr. Microstruct. Anal.
DOI 10.1007/s13632-017-0339-8

TECHNICAL ARTICLE

Analysis of the Cu-Al Milling Stages Through the Microstructure Evolution Studied by TEM and SEM

M. F. Giordana[1] · N. Muñoz-Vásquez[2] · M. R. Esquivel[1,3] · E. Zelaya[1]

Received: 3 November 2016 / Revised: 13 February 2017 / Accepted: 18 February 2017

Abstract Mechanical alloying of Cu-16 at.%Al and Cu-30 at.%Al was performed using both a planetary and a horizontal milling devices. The starting powders were high-purity Cu and Al. The different stages of milling were identified and characterized as initial, intermediate, final, and completion. The obtained microstructures were investigated by scanning electron microscopy and transmission electron microscopy. The evolution of the microstructure was studied considering the particle size variation. A decrease in the particle size was found as the Al content increases. The evolution of the nanostructure was studied considering the grain size variation. No marked changes on the nanostructure were detected during milling regardless either the type of mill used or composition selected. Mean grain sizes' values found were between 10 nm and 26 nm for each stage of milling. Power consumption of the milling process was calculated at laboratory scale to analyze the chances of a potential scaling up of the milling process. Starting aggregation state, microstructure and dominant phase changes, and evolution of mechanical alloying stages were considered. Performance of milling was compared to traditional high-temperature methods to compare the advantages and disadvantages of both synthesis methods.

✉ M. F. Giordana
giordana@ifir-conicet.gov.ar

[1] Centro Atómico Bariloche., CNEA-CONICET Av. Bustillo Km 9.5, 8400 Bariloche, Argentina

[2] Instituto Balseiro, Centro Atómico Bariloche, ANPCyT, Av. Bustillo 9500, 8400 Bariloche, Argentina

[3] Centro Regional Universitario Bariloche, Universidad Nacional del Comahue., 8400 Bariloche, Argentina

Keywords Mechanical alloying · Power consumption · Microstructure evolution · Cu-Al · TEM · SEM

Introduction

Nanostructured alloys became popular due to the enhancement of the properties compared to materials with conventional grain sizes [1–3]. Among these properties, it is worth to mention ductility, strength, and diffusion kinetics [4, 5]. Therefore, it is commercially attractive to develop synthesis methods of nanostructured materials [6–10]. Mechanical alloying (MA) is a well-known powder processing technique due to its simple know-how for the synthesis of alloys [11]. In particular, MA is especially useful in the production of alloys having constituents with a large difference in melting temperatures. Synthesis of nanostructured alloys is enhanced at low temperatures, $T < 423$ K ($T < 150$ °C) [12, 13]. Cold compact and hot rolling of pre-alloyed powders is one of the traditional processing routes used to obtain shape memory alloys. However, the properties of the final alloy depend on the microstructure of the initial powder. Therefore, it is important to analyze in detail the evolution of the micro- and nanostructures during milling [14, 15].

According to the composition, morphology, and microstructure, the MA synthesis process can be characterized as consisting in various stages. Benjamin and Volin [16] identified five different stages of alloying: particle flattening, welding predominance, equiaxed particle formation, random welding orientation, and steady-state processing. Recently, some authors divided the process into four different stages [17–19]: initial, intermediate, final, and completion. The MA consists in a cycle of fracture and cold welding, and the initial stage is controlled by fracture

Published online: 31 March 2017

process, without having a compositional homogeneity. The following stage is the intermediate which is controlled by both fracture and cold welding. At this stage, compositional changes are clearly evidenced. As milling continues, the formation of new structures is identified at the final stage. Finally, the completion stage occurs when changes no longer occur reaching an equilibrium between cold welding and fracture.

The synthesis of alloys of the Cu-Al-Ni system by MA was widely studied over the last decades [15, 20, 21]. However, synthesis process of Cu-Al by MA is not completely described as observed in the current and available literature. Moreover, the most studied compositions in the Cu-Al system are the ones with a large percentage of Al [22]. For composition values between Cu-16 at.%Al and Cu-30 at.%Al, this system is interesting because it can present shape memory properties. Cold compacting and hot rolling of a pre-alloy Cu-Al powder mixture can produce a shape memory alloy with a high transformation temperature value over 200 °C [23, 24]. Shape memory alloys can transform from one structure to the other without diffusion at a certain temperature or stress value. This martensitic transformation is also independent of grains size within certain composition ranges. However, grain size effects appear for grain sizes below some tens of micrometers, giving rise to a pronounced drop in the martensitic transformation temperature. Furthermore, other properties can be improved or deteriorated by the reduction in grain sizes below this value. For example, fracture strain seems to increase as the grain size decreases. Then, it is desirable to find a method to produce Cu-Al-Ni or Cu-Al alloys with a grain size smaller than a certain value, i.e., 30 μm according to Vajpai et al. [21]. On the contrary, the reduction in grain sizes below 100 μm generates a decrement in the starting temperature of the martensitic transformation. This behavior was observed for different alloys such as Cu-Zn-Al [25], Cu-Al-Be [26], and Cu-Al-Ni [27]. It becomes pronounced for grain sizes below 20 μm [26]. Thus, it can be worth to know the grain size of the alloy through the synthesis method selected. In the work of Samal et al. [28], an ultrafine Cu-25% wt. Al alloy was synthesized using a planetary ball mill. After 50 h of milling, they obtained a powder composed by particle with sizes around 200–400 nm. These particles contain a large number of grains with sizes around 15–20 nm.

The present work analyzes in detail the micro- and nanostructures of the powders as a further analysis of the results of a previous article [29]. The initial Cu and Al powders and the mechanically alloyed ones were consisted by particles with sizes in the micrometric scale. These particles were composed by a large number of nanometric grains. The evolution of the particle and grain sizes was studied for Cu-16 at.%Al and Cu-30 at.%Al alloys obtained by planetary and horizontal mills. Both types of milling are considered by Suryanarayana [11] as medium- and low-energy mills, respectively. Cu-Al system among others can turn amorphous by a high-energy mill [28, 30, 31]. One of the main objectives is to carefully study the microstructure evolution of Cu-Al system. For this reason, medium- and low-energy mills were chosen in this work. The powders were analyzed using scanning electron microscopy (SEM) and transmission electron microscopy (TEM). SEM was used to determine the evolution of the microstructure, while TEM allowed the study of nanostructured grains. The previous article consisted in a detailed study phase evolution during MA [29], while the aim of this work is to determine the nano- and microstructure evolution in order to establish the best composition and type of mill to develop a shape memory alloy with accurate grain sizes. This study characterizes the different stages of milling in the Cu-Al system between Cu-16 at.%Al and Cu-30 at.%Al, and it allows the estimation of the power consumption in order to scale up the process from laboratory to near-industrial level.

Materials and Methods

Elemental Cu (Sigma-Aldrich, 99.999% purity-5 mesh) and Al (Alfa Aesar, 99.5% purity-100 mesh) were used. Commercial powders were set with stainless steel balls in a stainless steel chamber under Ar atmosphere (99.999%). Figure 1a and b shows SEM micrographs of the high-purity initial Cu and Al powders, respectively. The mean grain diameter of the starting powders was equal to 15 ± 8 nm for Cu and 26 ± 15 nm for Al. Milling processes were performed at controlled conditions (humidity < 100 ppm, O_2 content < 5 ppm) for two different compositions of Cu-Al. The nominal compositions of the powders were Cu-16 at.%Al and Cu-30 at.%Al. The elemental blends were mechanically alloyed in two different devices with different conditions:

1. PM: planetary-motioned mill. The selected speed was 120 rpm. The ball/sample mass ratio was 8.25:1. The integrated milling times (t_{im}) were 10, 20, 30, and 50 h.
2. HM: horizontal mill. The selected speed was 140 rpm. The ball/sample mass ratio was 22.33:1. The integrated milling times (t_{im}) were 10, 30, 50, and 100 h.

The integrated milling time is the time the sample was effectively milled. The value does not include the time of removal of samples from mill or the time the mill inverts the direction of rotation. Figure 1c shows schematic representations of the mills functioning. HM reaches a global milling temperature below 150 °C [18]. PM reaches at the

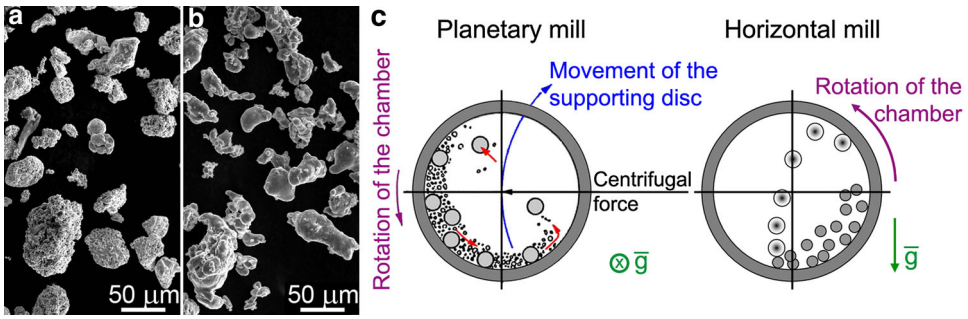

Fig. 1 SEM micrographs of the initial (**a**) copper and (**b**) aluminum powders. (**c**) Schematic representation of the functioning of PM and HM, vector g represents gravity direction

Table 1 Type of mill and milling time employed for each sample and general characteristics of SEM measurements

Composition: Cu-16 at.%Al				Composition: Cu-30 at.%Al			
Sample name	Type of mill	t_{im} (h)	Particle size (μm)	Sample name	Type of mill	t_{im} (h)	Particle size (μm)
16-PM-10	PM	10	127 ± 52	30-PM-10	PM	10	124 ± 46
16-PM-20	PM	20	80 ± 40	30-PM-20	PM	20	37 ± 17
16-PM-30	PM	30	80 ± 60	30-PM-30	PM	30	27 ± 19
16-PM-50	PM	50	103 ± 40	30-PM-50	PM	50	18 ± 12
16-HM-10	HM	10	135 ± 70	30-HM-10	HM	10	99 ± 42
16-HM-30	HM	30	167 ± 73	30-HM-30	HM	30	29 ± 26
16-HM-50	HM	50	239 ± 98	30-HM-50	HM	50	22 ± 21
16-HM-100	HM	100	173 ± 80	30-HM-100	HM	100	16 ± 10

selected conditions global temperature values below 200 °C. In neither case, the local temperature value, i.e., the instantaneous temperature reached during collision of balls against the sample, is known [11].

From now on, sample label briefly indicates the Al concentration, mill type, and milling time, e.g., 16-PM-10 stands for Cu-16 at.%Al milled in the planetary mill for 10 h. Table 1 presents the nomenclature.

Particle size and morphology were observed by a SEM FEI 515 microscope with an EDAX 9900 spectrometer for EDS analysis. Grain size was measured from TEM images acquired in a TEM FEI CM200 UT, operated at 200 kV. In order to obtain samples with adequate granulometry for TEM, the powders suspended in ethyl alcohol were manual mill by vertical smash in an agate mortar and some drops of the suspension were deposited onto an ultrathin holey carbon copper grid. The measurements of particle and grain sizes were performed from SEM images and TEM dark field micrographs, respectively. This task was carried out by assuming that the powders under study were circle-like shapes. Then, the characteristic magnitude was the diameter of the plane area. All measurements were performed using an image analysis software (iTEM Olympus Soft Imaging Solutions). Powders were also characterized by room-temperature x-ray diffraction, using a Philips PW 1710/01 and a PANalytical X'Pert diffractometers with Cu Kα radiation.

Results

Morphology of the Powders

The initial stage is controlled by fracture process [17–19]. The fracture process is clearly recognized in some of the particles presented in Fig. 2. Table 1 summarizes the experimental conditions of each sample shown in Fig. 2. Particularly, this process is observed at 10 h of milling. For example, it is presented a flake-like particle, in the micrograph of the sample 16-PM-10 as shown in Fig. 2a. Figure 2c corresponds to the sample 30-PM-10. A large particle with really straight cuts revealing also the occurrence of the fracture process is shown. Some particles of the samples milled by 10 h in HM have edges forming well-defined angles as shown by the arrows in Fig. 2b, d. In most of the micrographs corresponding to 10 h of milling, it is possible to find particles with rounded surfaces, which denotes the occurrence of cold welding. This morphology is related to the evolution from the initial to the intermediate stage. The rounded surfaces are the consequence of successive folding of layers. This behavior is similar to the observed one in the particle in the center of Fig. 2b. The intermediate stage is associated with the beginning of alloying. For the composition Cu-16 at.%Al, the intermediate stage takes place up to 20 and 30 h for PM and HM,

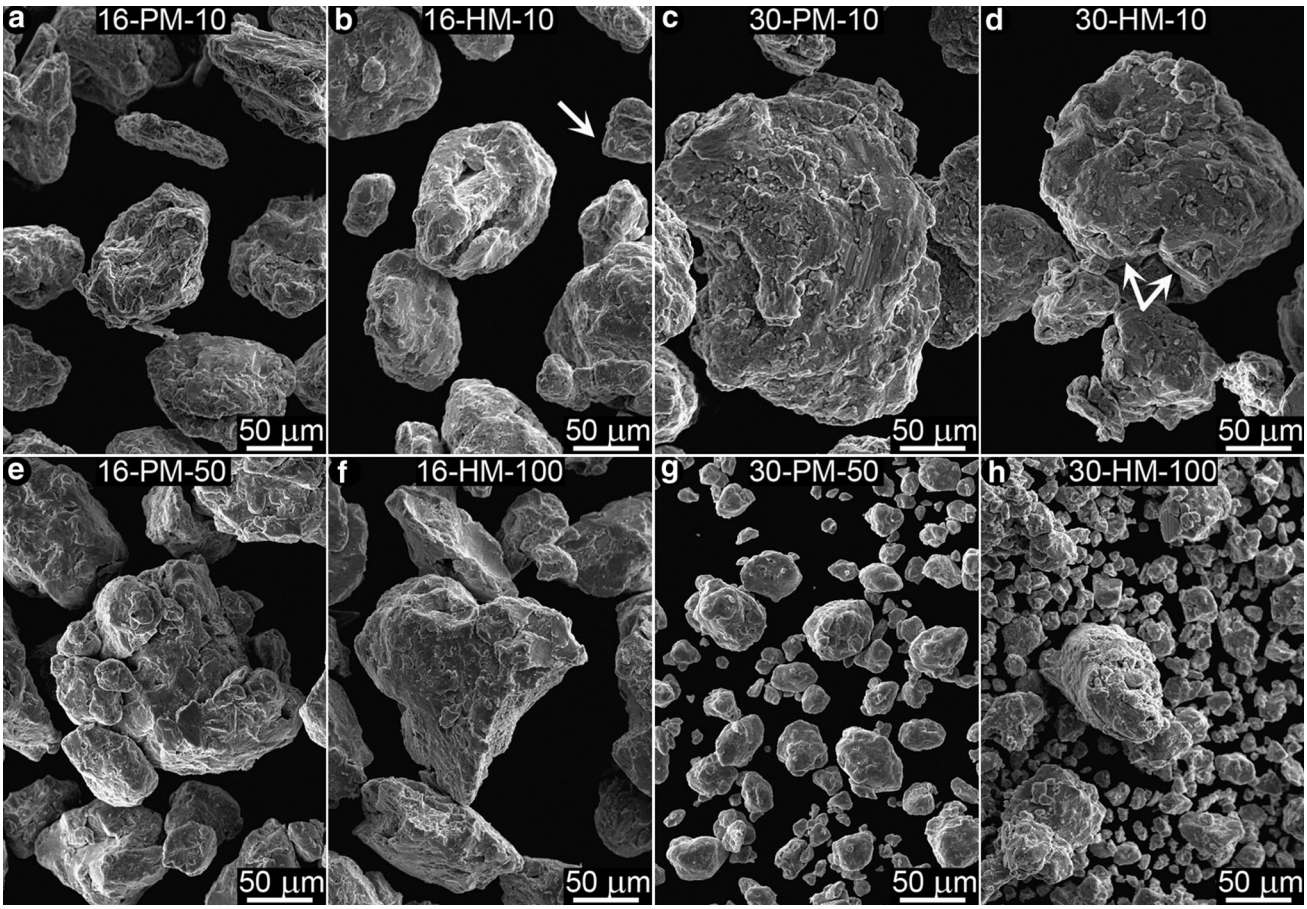

Fig. 2 SEM micrographs for the initial and completion milling steps. Micrographs are shown for each composition and type of mill. $t_{im} = 10$ h, 16 at.%Al, PM (**a**), HM (**b**), 30 at.%Al, PM (**c**), HM (**d**), 16 at.%Al, $t_{im} = 50$ h, PM (**e**), $t_{im} = 100$ h, HM (**f**), 30 at.%Al, $t_{im} = 50$ h, PM (**g**), $t_{im} = 100$ h, HM (**h**)

respectively. The beginning of the final stage is characterized by the formation of new phases [29].

No composition change occurs at longer milling times, and mechanical alloying simply evolves to mechanical milling. This milling condition is known as completion stage. At this stage, the predominance of the fracture over the cold welding depends on the way the systems relieve excess free energy of the surface. Samples obtained at the last step of each milling, 50 h for PM and 100 h for HM, could be related to the completion stage.

Figure 2e shows a representative image of the last step for the sample 16 at.%Al for PM. It depicts a large particle with rounded surface due to cold welding. Figure 2f shows sample obtained at 16-HM-100. It shows particles with flat surfaces and well-defined boundaries. This morphology is well related to fracture. The image also displays some other particles with rounded surfaces. Finally, the refinement of the structure of the powder from the micrographs of Fig. 2g, h is easily observed. These images correspond to 30 at.%Al milled for 50 h in PM and for 100 h in HM, respectively. The gradual decrement in the mean particle size is related to the completion stage slightly controlled by the fracture process.

Microstructural Evolution: Particle Size

Particle sizes were measured using SEM images. For each sample, at least 200 particles were measured. Figure 3 presents the histograms for samples obtained at the first and last stages of each milling process for each composition. The average values obtained for the particle size for each sample are shown in Table 1. The first stage related to 10 h is represented by columns with a tilted striped pattern. The last stage related to 50 h for PM or 100 for HM is represented by full gray columns.

Figure 3a shows the measurement results for the composition Cu-16 at.%Al milled in the planetary device. The mean value obtained for 16-PM-10 was equal to 127 µm, with a standard deviation of 52 µm, Table 1. For 16-PM-50, the mean value was equal to 103 µm and the standard deviation was equal to 40 µm. The results evidence the fact that no appreciable particle size variation was detected

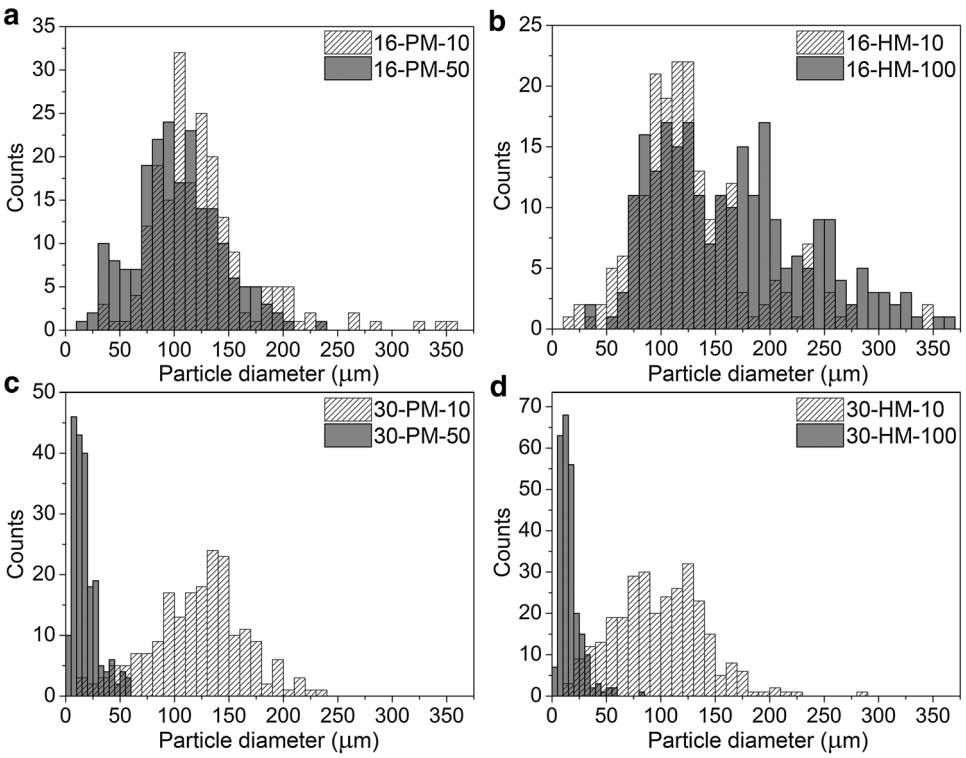

Fig. 3 Histograms representing the measurements of particle size of samples (**a**) 16-PM 10 and 50 h, (**b**) 16-HM 10 and 100 h, (**c**) 30-PM 10 and 50 h, (**d**) 30-HM 10 and 100 h

during milling. This fact is easily observed from the superposition of the distribution on both histograms. The particle size is also almost constant during milling for the case of the horizontal mill and for this composition. The measured value was equal to (135 ± 70) μm for 16-HM-10 and it was equal to (173 ± 80) μm for 16-HM-100 as shown in Fig. 3b. Consequently, considering the dispersion of the measurements, no significant particle size variation was observed. Intermediate milling times presented similar results as the first and last stages of each milling process.

In the case of the composition Cu-30 at.%Al, the evolution of the particle size was rather different than in the case of 16 at.%Al. The mean particle size was equal to (124 ± 46) μm after 10-h milling in the PM as shown in Table 1. Meanwhile, the mean value obtained for 30-PM-50 was equal to 18 μm with a standard deviation equal to 12 μm. The decrease in almost an order of magnitude in particle size is well represented by the histograms of Fig. 3c. Figure 3d shows the measurements performed in the samples 30-HM-10 and 30-HM-100. For these cases, the mean particle size value decreased from (99 ± 42) μm to (16 ± 10) μm, Table 1. A marked difference in the evolution of particle sizes appeared between the two compositions studied. The refinement in particles sizes seems to be dependent on the Al content. A possible reason to this difference is discussed in "Micro/nanostructure evolution" section.

The mean diameters for each step and mill are represented in Fig. 4. It is done to study in detail the evolution of the particle size for the composition Cu-30 at.%Al. The values obtained for the intermediate samples were: 37 ± 17 μm (30-PM-20), 27 ± 19 μm (30-PM-30), 29 ± 26 μm (30-HM-30), 22 ± 21 μm (30-HM-50) as summarized in Table 1. As a guide to the eye, two different curves were fitted. The gray one corresponds to PM, and the black one to HM. These curves are exponential functions. For the second stage of milling, 20 h (PM) and 30 h (HM), the mean particle size reached a value similar to the one obtained in the completion stage. The early decay of the values demonstrates the rapid evolution of this parameter for the composition Cu-30 at.%Al.

Nanostructural Evolution: Grain Size

All samples were powders composed of micrometric particles containing a large amount of nanometric grains. This parameter was studied by dark field (DF) images obtained from TEM. The determination of mean grain diameter was performed from DF micrographs. It is represented in Fig. 5.

Figure 5a shows the results obtained for the composition Cu-16 at.%Al for both mills. In the case of PM (full gray rhombus), the smallest mean value measured was equal to (12 ± 5) nm for the sample 16-PM-30. The largest value

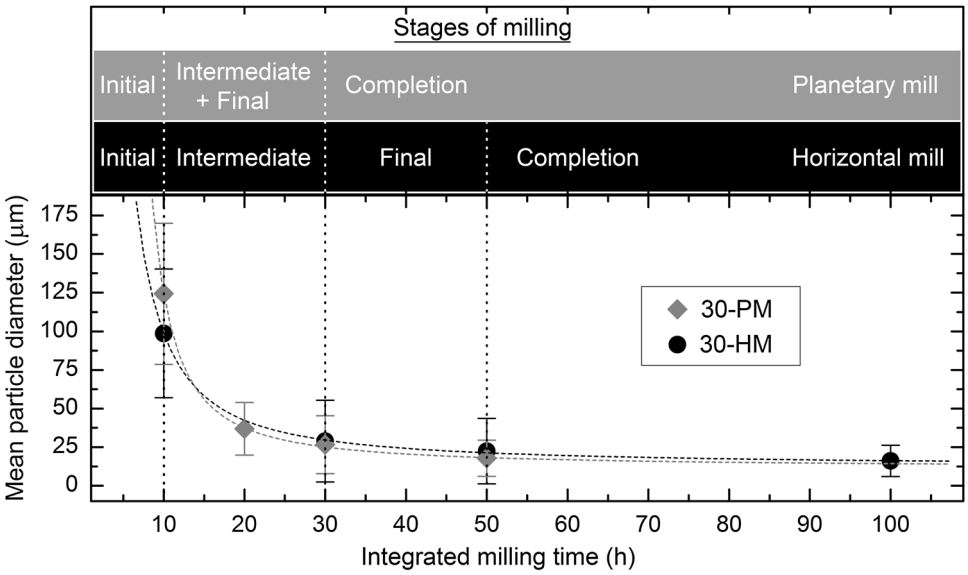

Fig. 4 Evolution of the mean particle diameter of the samples with a composition Cu-30 at.%Al. Stages of milling are schematically represented

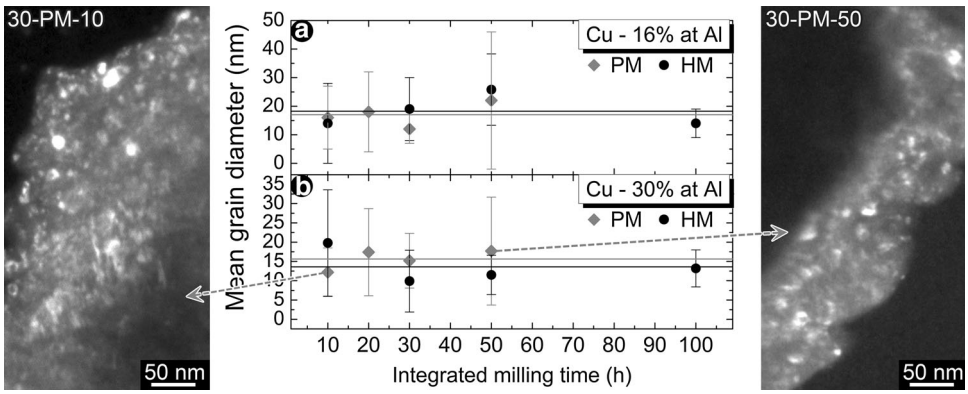

Fig. 5 Evolution of the mean grain diameter. (**a**) Cu-16 at.%Al, (**b**) Cu-30 at.%Al. Left and right pointed dark field images correspond to samples 30-PM-10 and 30-PM-50, respectively

was obtained at the last stage of the milling, and it was equal to (22 ± 24) nm. The other two values were in between these ones. It is possible to assure that no evolution was observed for this parameter during the milling considering the standard deviation of each measurement. This fact is represented in gray line in the figure by a zero-order polynomial function equal to the average value of the fourth measured diameters. The average value was equal to 17 nm. The zero-order polynomial function did not stand for all points, but it is within the error line values. A similar behavior was observed for the sample synthesized in the HM (full black circles). In this case, mean grain diameter values were between (14 ± 14) nm and (26 ± 13) nm. The zero-order polynomial function (black line) was equal to 18 nm.

The values obtained for the composition Cu-30 at.%Al are shown in Fig. 5b. The mean value obtained for the sample 30-PM-10 was equal to (12 ± 6) nm. This value was the smallest one found for samples milled in PM. The largest one was obtained for the last stage of the milling, being equal to (18 ± 14) nm. Both values are represented by the DF micrographs presented in Fig. 5. The DF image to the left corresponds to samples 30-PM-10. The DF image to the right corresponds to samples 30-PM-50. The comparison of both DF images showed no appreciable evolution of the grain sizes occurred during the milling. The plotted line that represents this fact had a constant value equal to 15.5 nm. Similar results were obtained for HM. The smallest mean grain diameter measured was equal to (10 ± 8) nm. The largest value was measured for the first stage of the milling, being equal to (20 ± 14) nm. The average value of the fourth measured diameters was equal to 13.5 nm. It is worth to mention that grain sizes were also measured for the initial powders. The mean grain diameter obtained was equal to (15 ± 8) nm for Cu, and it was equal to (26 ± 15) nm for Al.

Phase Evolution of the Powders

The different samples were characterized by XRD. Phases presented at each t_{im} were identified using the diffractograms. Figure 6 presents the diffractograms obtained for

the samples at the first and last stages of each milling for each composition. A summary of the detected phases by XRD for all samples is also presented [29]. The first stage of each milling is represented by full gray diffractograms, while the last stage is represented by black line curves.

Figure 6a, b shows the results obtained for samples with composition 16 at.%Al. For 10 h in both mills, XRD patterns show the presence of Cu and Al disaggregated [29], i.e., that Cu and Al elements could be identified separately in the XRD profile. For the last stages of each milling, the intermetallic detected for Cu-16 at.%Al was the stable phase according to the phase diagram [23]. The cubic α phase was obtained using both milling devices [29]. This final phase was reached at 30 h in both cases [29], Fig. 6c. As it is shown in Fig. 6d, e, XRD corresponding to 10-h milling of the samples with composition 30 at.%Al could be indexed considering the presence of Cu and Al [29]. On the contrary, the final intermetallic observed for Cu-30 at.%Al was not in total agreement with the equilibrium phase diagram. The planetary mill produced a mixture of α and γ_2 phases from 20-h milling [29] as presented in Fig. 6f. The horizontal mill produced γ_2 phase from 50-h milling [29]. At $t_{im} = 30$ h a mixture of α and γ_2 was detected [29] as shown in Fig. 6f.

Discussion

Stages of Milling

Stages of milling are analyzed in detail considering the morphology of both powders and phase stability. These characteristics are easily correlated with the effects of fracture and cold welding, the ones dominating the stages of mechanical alloying. For the composition Cu-30 at.%Al, the different milling stages are schematically represented in Fig. 4.

Initial Stage

The first stage of each milling is mainly controlled by the fracture process. Usually during this stage, the initial components remained without alloying with no evidence of cold welding. This behavior was clearly observed during the first 10 h of milling for PM and HM and for both compositions. After this first stage, the powders were composed only by initial Cu and Al in each sample [29], Fig. 6. The fracture process is also evidenced for particles with well-defined angles and remarkable straight lines in the surface.

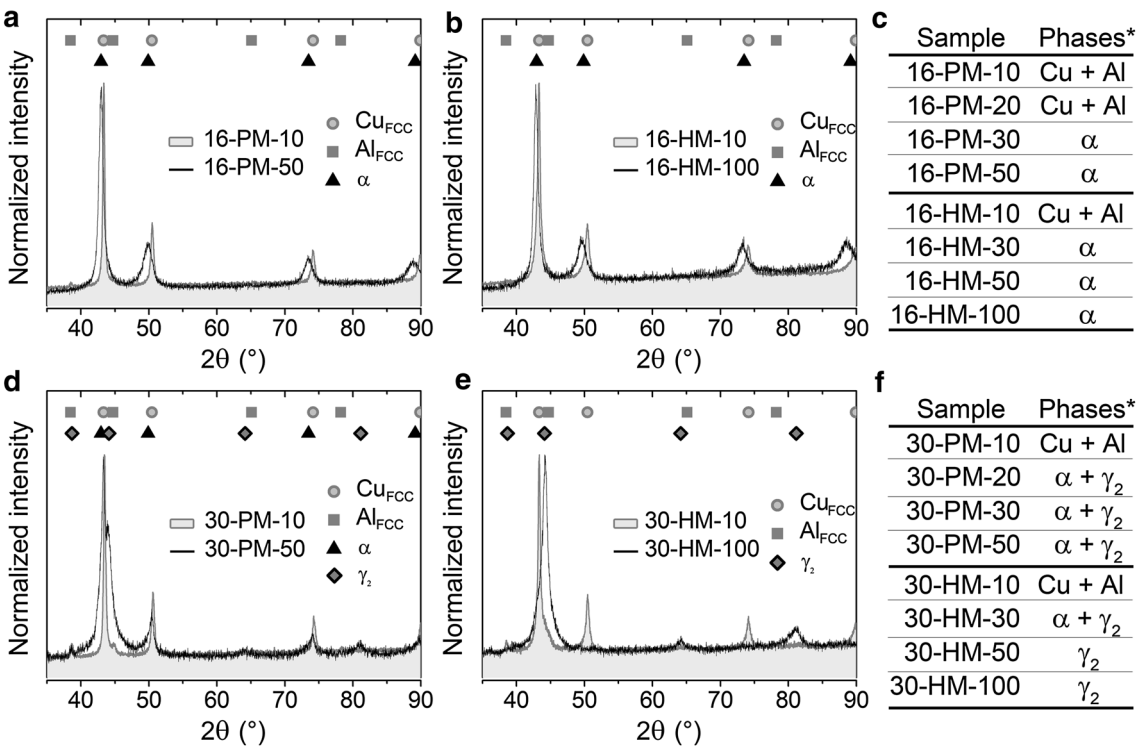

Sample	Phases*
16-PM-10	Cu + Al
16-PM-20	Cu + Al
16-PM-30	α
16-PM-50	α
16-HM-10	Cu + Al
16-HM-30	α
16-HM-50	α
16-HM-100	α

Sample	Phases*
30-PM-10	Cu + Al
30-PM-20	α + γ_2
30-PM-30	α + γ_2
30-PM-50	α + γ_2
30-HM-10	Cu + Al
30-HM-30	α + γ_2
30-HM-50	γ_2
30-HM-100	γ_2

Fig. 6 X-ray diffractograms of (**a**) 16-PM-10 and 16-PM-50, (**b**) 16-HM-10 and 16-HM-100, (**d**) 30-PM-10 and 30-PM-50, (**e**) 30-HM-10 and 30-HM-100. Summaries of the detected phase for Cu-16 at.%Al and Cu-30 at.%Al are presented in (**c**) and (**f**), respectively. *Asterisks* indicate phase identities reported previously [29]

Intermediate Stage

The second stage is related to the beginning of alloying. The alloying of powders is produced by the cold welding process. Figure 2a-d shows the particles obtained after 10-h milling. These particles presented rounded surfaces due to the successive folding of layers. The beginning of the intermediate stage is associated with rounded surfaces produced by cold welding. This fact is in agreement with the formation of new phases in each sample at the next stage of milling (30 h for 16-PM, 20 h for 30-PM and 30 h for HM) [29]. It is shown in Fig. 6c, f. For the composition Cu-30 at.%Al, the evolution of the mean particle size took place at this stage of milling as shown in Fig. 4.

Final Stage

The third stage starts when the final product appears and lasts until its total formation. This stage elapses from 20 to 30 h of milling for the sample 16-PM. The formation of the α phase was detected by transmission electron microscopy at 20-h milling [29]. The powder was composed only by the equilibrium phase at 30-h milling, Fig. 6c. After that, no new phases were detected. In the case of 16-HM, the final stage could occur between 10 and 30 h of milling. No clear distinction is observed between this and the intermediate stage. A similar behavior was observed for the sample 30-PM. As it is shown in Fig. 4, no clear distinction between the intermediate stage and the final stage is observed. Both stages occurred between 10 h and 30 h of milling. It happened because the starting of alloying was observed and the final product was obtained during this 20 h. In the 30-HM case, the final stage could be located at times longer than 50 h of milling where the only phase detected was γ_2 [29] as displayed in Fig. 6e, f.

Completion Stage

Compositional changes should not be observed at this last stage of milling. Then, this stage was considered as mechanical milling without alloying. The system evolved to the most energetically favorable situation. For samples with composition Cu-16 at.%Al, powders at the completion stage presented similar morphology as those ones observed at 30 h for PM and at 50 h for HM. This meant that it was unnecessary to mill any longer because no appreciable evolution was observed after the end of the final stage. A similar condition was observed for the composition Cu-30 at.%Al. After the final stage, no changes were detected.

Micro/Nanostructure Evolution

The evolution during milling of the powder microstructure depended on the initial composition of the blend. The mean particle diameter of the samples synthesized either by PM or by HM did not present appreciable variation for the composition Cu-16 at.%Al. During each milling process, particle sizes were around 140 μm. Histograms corresponding to $t_{im} = 10$ h were similar to the ones corresponding to the last stage of each milling process as observed in Fig. 3a, b. As shown in Fig. 4, the mean size of the particles decreased, as the milling time increased for the composition Cu-30 at.%Al. The decrement is highly pronounced during the intermediate stage of milling. Mean particle diameter was reduced from (124 ± 46) μm to (18 ± 12) μm for PM and from (99 ± 42) μm to (16 ± 10) μm for HM. In each case, the decrement was near one order of magnitude. These results reveal a decrease in the particle size as the Al content increases.

The large difference between the behaviors of both compositions could be attributed to the phases occurring in each case. For Cu-16 at.%Al, only α phase was detected after the beginning of alloying [29]. The α phase, the stable phase according the phase diagram [23], presents the same space group than Cu with a slightly larger lattice parameter due to the Cu substitutional replacement by a larger Al atom [32]. For Cu-30 at.%Al, in addition to the α phase, γ_2 phase was also detected [29]. The mass evolution of α and γ_2 phases according to Rietveld results was presented in [29]. The increase in the average mass percentage of γ_2 phase occurred as expense of the decrease in the average mass percentage of α phase. The unit cell of the γ_2 phase contained a total of 52 atoms and 2 structural vacancies with a lattice parameter three times larger than the one of α [33]. Therefore, the decrease in the particle size as the Al content increased could be attributed to the increase in the γ_2 phase. This conclusion is based on the idea that γ_2 phase is more fragile than the α one. It was also reinforced by the previous results obtained for a composition Cu-24 at.%Al [34]. In this case, a mixture of α and γ_2 phases was detected forming the final intermetallic [29]. The mean particle size of Cu-24 at.%Al was smaller than Cu-16 at.%Al and larger than Cu-30 at.%Al at the final stages of milling. A large decrease in particle size was reported for the Cu-Al-Mn system [35]. Amini et al. found that the mean particle size was reduced from 140 μm after 12 h of milling to 38 μm after 48 h of milling in a planetary device.

In opposite to the microstructure evolution, the powder nanostructure did not markedly evolve during milling in any of the studied cases. Mean grain sizes were between 10 and 26 nm for each stage of milling regardless type of

Table 2 Power consumption according to t_{im} and selected annealing conditions ($T = 1060$ °C during 1 h)

Sample name	t_{im} (h)	Power consumption by MA (kWh)	Power consumption by annealing (kWh)
16-HM-10	10	2.2	4.0
16-HM-30	30	6.6	4.0
16-HM-50	50	11.0	4.0
16-HM-100	100	22.0	4.0
30-HM-10	10	2.2	4.0
30-HM-30	30	6.6	4.0
30-HM-50	50	11.0	4.0
30-HM-100	100	22.0	4.0

mill or composition. These mean values, considering their dispersions, were also between the ones obtained for the initial Cu and Al powders. Therefore, the final grain size seems to be conditioned by the grain sizes of the initial particles for the systems studied in this work. A decrease in grain sizes was observed for other systems. For example, Samal et al. [28] study Cu-Al in a composition between the ones studied in this work using a high-energy mill. They measured the grain sizes by an indirect method using x-ray diffractograms. The mean value decreased from 21 nm to 6 nm after 10-h milling. The final particle sizes observed were near a hundred of nanometers. This value is much lower than the ones obtained in this work using low- and medium-energy mill devices. Zelaya et al. [13] reported a decrement in the grain sizes during the synthesis of Ni-Al by low-energy mechanical alloying. The same behavior of the grain size was reported by Chen et al. [4], using a high-energy ball mill in the same Ni-Al system. The lack of similarity between the Cu-Al system and other system can be attributed to the different ductile brittle balance of the phases synthesized during milling stages.

Many authors reported martensitic transformation after heat and mechanical treatment of the compacted powders [20]. However, only few works related the grain size of the powders and the grain size of the final alloy. Moreover, these few works only reported the initial particle size and they associated these values with the final grain size [15, 21]. They reported the highest fracture stress on Cu-Al-Ni system starting the manufactured process with powder particles around 20 μm. Due to this correlation, the optimum process for Cu-Al system seems to be with the planetary mill after 30 h of milling of Cu-30 at.%Al or the horizontal mill after 50 h of milling of Cu-30 at.%Al. Both processes produced particles that could increase the average fracture stress and could not generate a pronounced decrement in the starting temperature of the martensitic transformation [15, 21, 26]. Moreover, both milling times reached the final milling stage. However, the final manufactured of the Cu-Al alloy should be done using different grain sizes in the initial constituents in order to verify that correlation is still effective in Cu-Al system.

Mechanical Alloying Evolution and Power Consumption: A Roadmap to Scale up the Process

A viewpoint of the effectiveness of the MA process could be inferred from the power consumption occurred during processing. This performance was associated with integrated milling time (t_{im}), Table 2. In turn, it was correlated with the evolution of the microstructure, the time elapsed in each milling stage, and the microstructure and identity of the final products.

Horizontal mill is selected for this study because it is homologous to those used in ceramic industry at large scale. In addition, it should be pointed out that HM is more efficient than PM for Cu-30 at.%Al, since the final equilibrium phase was obtained faster in the HM mill [29]. The t_{im} necessary to reach the final product is selected as the variable of the process. In each case, values are compared to those needed to synthesize and equivalent Cu-Al sample by fusion methods. The conditions selected were 1333 K (1060 °C) and 1 h under Ar atmosphere. This is considered a minimum amount of time to allow the diffusion of constituents to form the selected alloys for Cu-Al. In each case, the power consumption was calculated from devices used at laboratory scale.

For 16-HM sample the power consumption value to reach the final phase is between 2.2 and 6.6 kWh. The value corresponds to t_{im} between 10 and 30 h because between these values the final stage of milling was achieved. Milling for longer times neither change the identity of the final α phase nor the particle size distribution nor the morphology, and therefore, it is a waste of energy. The value is similar to the power consumption obtained by equilibrium methods. Nevertheless, the last one requires a detailed control of the Al content due to differential volatilization. Closed controlled systems and high-temperature materials are needed to achieve these treatments.

For 30-HM sample, the power consumption needed is between 6.6 and 11 kWh. The value corresponds to t_{im} values between 30 and 50 h. In this case final phase achieved is γ_2 and it was reached between these two t_{im} values. Milling for longer times is only required if a narrow

particle size distribution is needed for the final product as deduced from Fig. 3d. Compared to fusion method, the energy consumption is higher. Nevertheless, Al differential evaporation should be also controlled in this case. This control is not needed in this MA process because temperature of operation is lower than 423 K (<150 °C).

In each case, if time of annealing is extended to 2 h the energy consumption values duplicate. Only 10 h of annealing is needed to reach maximum energy consumption by MA. Then, the best synthesis method should be selected from a careful study that considers equilibrium between equipment capable of working at either 1273 K (1000 °C; fusion) or 423 K (150 °C; MA) and energy consumption.

Conclusions

Powders of Cu and Al were milled with proportions equal to 16 and 30 at.%Al, using a planetary and an horizontal mills. Particle size and morphology were observed by scanning electron microscopy. Four stages of milling were characterized as a function of the integrated milling time. Nanostructure evolution was studied considering the evolution of grain size. It was measured from transmission electron microscopy images.

Initial stage ranged from 0 to 10 h regardless type of mill or composition. The next stages could be clearly distinguished only in two cases, for Cu-16 at.%Al milled in the planetary device and for Cu-30 at.%Al milled in the horizontal device. In the first one, the intermediate stage elapses from 10 to 20 h, the final stage from 20 to 30 h, and the completion stage occurred at integrated times longer than 30 h. In the second one, the intermediate stage was at integrated times between 10 and 30 h, the final stage was between 30 and 50 h, and then, the completion stage took place after 50 h of milling. The intermediate and final stages could not be separated in the other two cases, i.e., Cu-16 at.%Al milled in the horizontal device and Cu-30 at.%Al milled in the planetary device. These stages occur simultaneously during the milling.

The microstructure evolution depends on the initial composition of the blend. The mean particle diameter did not present appreciable variations for the composition Cu-16 at.%Al. On the contrary, the mean size of the particles decreased, as the milling time increased for the composition Cu-30 at.%Al. We conclude that the decrease in the particle size occurred as the Al content increases. Mean grain sizes were between the ones obtained for the initial Cu and Al powders. No evolution was detected regarding the nanostructure. The final grain size seems to be conditioned by the grain sizes of the initial particles for the systems studied in this work.

MA process main consumption variable, t_{im}, is strictly related to the time elapsed to reach final stage. On the contrary, high-temperature methods' variables are both time and temperature of annealing. Then, the roadmap to the scale up of the MA process to industrial level should consider carefully investment in both equipment and energy consumption.

Acknowledgments The authors express their thanks to Consejo Nacional de Investigaciones Científicas y Técnicas (CONICET), to Agencia Nacional de Promoción Científica y Tecnológica (ANPCyT: PICT-2011-0643 and PICT-2011-0092), and to Comisión Nacional de Energía Atómica (CNEA) for supporting this work.

References

1. K. Kumar, H. Van Swygenhoven, S. Suresh, Mechanical behavior of nanocrystalline metals and alloys. Acta Mater. **51**, 5743–5774 (2003). doi:10.1016/j.actamat.2003.08.032
2. X. Mao, D. Li, Z. Wang, X. Zhao, L. Cai, Surface nanocrystallization by mechanical punching process for improving microstructure and properties of Cu30Ni alloy. Trans. Nonferrous Met. Soc. China **23**, 1694–1700 (2013). doi:10.1016/S1003-6326(13)62650-3
3. M. Izadinia, K. Dehghani, Structure and properties of nanostructured Cu-13.2Al-5.1Ni shape memory alloy produced by melt spinning. Trans. Nonferrous Met. Soc. China **21**, 2037–2043 (2011). doi:10.1016/S1003-6326(11)60969-2
4. T. Chen, J.M. Hampikian, N.N. Thadhani, Synthesis and characterization of mechanically alloyed and shock-consolidated nanocrystalline NiAl intermetallic. Acta Mater. **47**(8), 2567–2579 (1999). doi:10.1016/S1359-6454(99)00059-2
5. M. Slimi, M. Azabou, L. Escoda, J.J. Suñol, M. Khitouni, Structural and microstructural properties of nanocrystalline Cu–Fe–Ni powders produced by mechanical alloying. Powder Technol. **266**, 262–267 (2014). doi:10.1016/j.powtec.2014.03.064
6. Y. Chen, Q. Wang, J. Lin, M. Liu, J. Hjelen, H.J. Roven, Grain refinement of magnesium alloys processed by severe plastic deformation. Trans. Nonferrous Met. Soc. China **24**, 3747–3754 (2014). doi:10.1016/S1003-6326(14)63528-7
7. R.Z. Valiev, T.G. Langdon, Principles of equal-channel angular pressing as a processing tool for grain refinement. Prog. Mater Sci. **51**, 881–981 (2006). doi:10.1016/j.pmatsci.2006.02.003
8. M.K. Nazemi, S. Sheibani, F. Rashchi, V.M. Gonzalez-DelaCruz, A. Caballero, Preparation of nanostructured nickel aluminate spinel powder from spent NiO/Al_2O_3 catalyst by mechanochemical synthesis. Adv. Powder Technol. **23**, 833–838 (2012). doi:10.1016/j.apt.2011.11.004
9. V. Umapathy, A. Manikandan, S. Arul Antony, P. Ramu, P. Neeraja, Structure, morphology and opto-magnetic properties of Bi2MoO6 nano-photocatalyst synthesized by sol–gel method. Trans. Nonferrous Met. Soc. China **25**, 3271–3278 (2015). doi:10.1016/S1003-6326(15)63948-6
10. Z. Tan, K. Sato, S. Ohara, Synthesis of layered nanostructured TiO_2 by hydrothermal method. Adv. Powder Technol. **26**, 296–302 (2015). doi:10.1016/j.apt.2014.10.011
11. C. Suryanarayana, Mechanical alloying and milling. Prog. Mater Sci. **46**, 1–184 (2001). doi:10.1016/S0079-6425(99)00010-9
12. S.K. Pabi, B.S. Murty, Mechanism of mechanical alloying in NiAl and CuZn systems. Mater. Sci. Eng., A **214**, 146–152 (1996). doi:10.1016/0921-5093(96)10224-0

13. E. Zelaya, M.R. Esquivel, D. Schryvers, Evolution of the phase stability of Ni–Al under low energy ball milling. Adv. Powder Technol. **24**, 1063–1069 (2013). doi:10.1016/j.apt.2013.03.008
14. S. Pourkhorshidi, N. Parvin, M.S. Kenevisi, M. Naeimi, H. Ebrahimnia Khaniki, A study on the microstructure and properties of Cu-based shape memory alloy produced by hot extrusion of mechanically alloyed powders. Mater. Sci. Eng., A **556**, 658–663 (2012). doi:10.1016/j.msea.2012.07.044
15. S.K. Vajpai, R.K. Dube, S. Sangal, Application of rapid solidification powder metallurgy processing to prepare Cu–Al–Ni high temperature shape memory alloy strips with high strength and high ductility. Mater. Sci. Eng., A **570**, 32–42 (2013). doi:10.1016/j.msea.2013.01.063
16. J.S. Benjamin, T.E. Volin, The mechanism of mechanical alloying. Metall. Trans. **5**, 1929–1934 (1974)
17. L. Lu, M.O. Lai, *Mechanical alloying*, vol. 4 (Kluwer Academic Publishers, Boston, 1998)
18. M.N. Ceron Hurtado, M.R. Esquivel, Stages of mechanical alloying during the synthesis of Sn-containing AB_5-based intermetallics. Int. J. Hydrogen Energy **35**, 6057–6062 (2010). doi:10.1016/j.ijhydene.2009.12.072
19. S.A. Obregón, J.J. Andrade-Gamboa, M.R. Esquivel, Synthesis of Al-containing $MmNi_5$ by mechanical alloying: milling stages, structure parameters and thermal annealing. Int. J. Hydrogen Energy **37**, 14972–14977 (2012). doi:10.1016/j.ijhydene.2012.01.170
20. S.M. Tang, C.Y. Chung, W.G. Liu, J. Mater. Process. Technol. **63**, 307–312 (1997). doi:10.1016/S0924-0136(96)02641-6
21. S.K. Vajpai, R.K. Dube, S. Sangal, Microstructure and properties of Cu–Al–Ni shape memory alloy strips prepared via hot densification rolling of argon atomized powder preforms. Mater. Sci. Eng., A **529**, 378–387 (2011). doi:10.1016/j.msea.2011.09.046
22. A. Evirgen, M.L. Öveçoğlu, Characterization investigations of a mechanically alloyed and sintered Al–2 wt%Cu alloy reinforced with WC particles. J. Alloys Compd. **496**, 212–217 (2010). doi:10.1016/j.jallcom.2010.02.136
23. M.A. Dvorack, N. Kuwano, S. Polat, H. Chen, C.M. Wayman, Decomposition of β_1-phase Cu–AI–Ni alloy at elevated temperature. Scripta Metall. **17**(11), 1333–1336 (1983)
24. M. Ahlers, Martensite and equilibrium phases in Cu–Zn and Cu–Zn–Al alloys. Prog. Mater Sci. **30**, 135–186 (1986)
25. W. Jianxin, J. Bohong, T.Y. Hsu, Influence of grain size and ordering degree of the parent phase on M_S in a Cu–Zn–Al Alloy containing boron. Acta Metall. **36**, 1521–1526 (1988)
26. P.M. La Roca, L.M. Isola, C.E. Sobrero, Ph Vermaut, J. Malarría, Grain size effect on thermal-induced martensitic transformation of polycrystalline Cu-based shape memory alloys. Mater. Today: Proc. **2**(3), 743–746 (2015). doi:10.1016/j.matpr.2015.07.389
27. K. Mukunthan, L.C. Brown, Preparation and properties of fine grain β-CuAlNi strain- memory alloys. Metall. Trans. A **19**, 2921–2929 (1988)
28. S. Samal, B. Satpati, D. Chaira, Production and dispersion stability of ultrafine Al–Cu alloy powder in base fluid. J. Alloys Compd. **504S**, 389–394 (2010). doi:10.1016/j.jallcom.2010.03.223
29. M.F. Giordana, M.R. Esquivel, E. Zelaya, A detailed study of phase evolution in Cu–16 at.%Al and Cu–30 at.%Al alloys under different types of mechanical alloying processes. Adv. Powder Technol. **26**, 470–477 (2015). doi:10.1016/j.apt.2014.12.005
30. D.V. Dudina, O.I. Lomovsky, K.R. Valeev, S.F. Tikhov, N.N. Boldyreva, A.N. Salanov, S.V. Cherepanova, V.I. Zaikovskii, A.S. Andreev, O.B. Lapina, V.A. Sadykov, Phase evolution during early stages of mechanical alloying of Cu–13 wt% Al powder mixtures in a high-energy ball mill. J. Alloys Compd. **629**, 343–350 (2015). doi:10.1016/j.jallcom.2014.12.120
31. G. Gonzalez, A. Sagarzazu, D. Bonyuet, L. D'Angelo, R. Villalba, Solid state amorphisation in binary systems prepared by mechanical alloying. J. Alloys Compd. **483**, 289–297 (2009). doi:10.1016/j.jallcom.2008.08.127
32. P.R. Swann, H. Warlimont, The electron-metallography and crystallography of copper-aluminum martensites. Acta Metall. **11**(6), 511–527 (1963)
33. S. Westman, Refinement of the γ-Cu9Al4 Structure. Acta Chem. Scand. **19**, 1411–1419 (1965)
34. M.F. Giordana, N. Muñoz-Vásquez, M. Garro-González, M.R. Esquivel, E. Zelaya, Study of the formation of Cu-24at.%Al by reactive milling, Procedia. Mater. Sci. **9C**, 262–270 (2015). doi:10.1016/j.mspro.2015.04.033
35. R. Amini, S.M.M. Mousavizad, H. Abdollahpour, M. Ghaffari, M. Alizadeh, A.K. Okyay, Structural and microstructural phase evolution during mechano-synthesis of nanocrystalline/amorphous CuAlMn alloy powders. Adv. Powder Technol. **24**, 1048–1053 (2013). doi:10.1016/j.apt.2013.03.005